Correct calculation of nitrogen charge state passing through highly ionized carbon plasmas

Manuel D. Barriga-Carrasco and José Vázquez-Moyano
E.T.S.I. Industrial, Universidad de Castilla-La Mancha, E-13071 Ciudad Real, Spain

(Received 11 August 2020; revised 1 July 2021; accepted 1 July 2021; published 30 July 2021)

In the present work, we reanalyze the energy loss experimental data from Cayzac *et al.* [Nat. Commun. **8**, 15693 (2017)] using our successful ion charge state theoretical model. We predict lower nitrogen charge values, from 3.5+ to 5.0+, than the ones calculated by Cayzac *et al.*, fitting better to their data. For energy loss estimations, we use the same stopping model, so our predictions agree better with the experimental data only due to our charge state model. Different projectile electron loss and capture processes are taken into account to estimate the projectile charge state. The projectile electron loss, or ionization, with plasma ions and free electrons are considered. On the other hand, the projectile electron capture, or recombination, with plasma free or bound electrons are also considered. The projectile ionization with plasma ions is shown as the main factor that modifies the mean charge of the projectile. Here, the new Kaganovich fitting formula for this projectile ionization is used because it seems to be more accurate than Gryzinsky's fitting in the low energy range. Our charge state model fits better with experimental data than any other model in the bibliography. Thus, it should be considered in any charge state and any energy loss estimation to obtain reliable results in future work.

DOI: 10.1103/PhysRevE.104.015217

I. INTRODUCTION

The aim of the work of Cayzac *et al.* [1] was the experimental discrimination of ion stopping models near the Bragg peak in highly ionized carbon plasmas. The Bragg peak is where it is supposed that the stopping reaches its maximum, which makes it easier to discriminate these stopping models. For this purpose, they chose as ions the lightest projectiles available to them at that moment. Light ions simplify the beam charge distribution in the stopping power calculation as stopping depends approximately quadratically on the projectile charge.

The experiment was carried out at GSI-Darmstadt, Germany, in which two high-energy lasers, PHELIX and NHELIX [2], were used to create the plasma that was later probed with the pulsed ion beam from the UNILAC accelerator. The plasma was created by heating a 100 μg cm^{-2} carbon foil from both sides by the two laser beams, leading to full target ionization after 6–7 ns with free electron densities of $n_e \approx 5 \times 10^{20}$ cm^{-3} and electron temperatures of $T \approx 150$ eV [3,4]. The plasma conditions were simulated with the two-dimensional (2D) hydrodynamic code RALEF2D [5] for the times $t = 0$–15 ns after the beginning of the target heating. Then, the plasma ionization is deduced by postprocessing the density [6] and temperature profiles with the FLYCHK code [7], which determines the free electron density profile in nonlocal-thermodynamic-equilibrium (NLTE) state, the common state of a laser plasma [8].

The nitrogen ions passed through a degrader before interacting with the carbon plasma to reduce the beam energy to $E_0 = 0.586$ MeV/u. The degraders had a density $\rho = 1.84$ g cm^{-3} and were produced by rolling carbon foils down to a thickness close to 41 μm. Due to its thickness, the outgoing ion beam is in its mean charge state. The degrader was positioned 15 mm in front of the target, which both ensures a free path for the heating lasers and limits the transverse broadening due to angular scattering of the ion beam when probing the plasma. In addition, the degrader was systematically destroyed by the plasma emission and expansion from the target and had to be changed after each shot.

The energy loss of the nitrogen ions was measured by a time of flight (TOF) detector based on 10 identical polycrystalline chemical vapor deposition (CVD) diamond samples. The total detection area of 166 mm^2 was large enough to collect about 20% of the ions at the beam focus position, which guarantees sufficient signal amplitudes for a quantitative energy-loss analysis. Cayzac *et al.* compared this experimental energy loss data with the predictions of the Li-Petrasso (LP) stopping model [9], which represents a perturbative scheme, and with the predictions of the T-Matrix (TM) stopping model by employing a velocity-dependent screening length [10], which includes a detailed treatment of close binary collisions as well as quantum diffraction effects.

To predict the projectile charge state, they used a Monte Carlo code based on cross sections to calculate the mean beam charge [3,4], as well as the mean charge state models by Kreussler [11–13] and Gus'kov [14]. Finally, they combined these three charge state models with the LP and TM stopping models in order to simulate and compare the energy loss of the beam with the data. They conclude that TM and Gus'kov models enable their estimations to better suit the experimental data.

Here in this work, we present our charge state model that fits much better to their experimental data.

II. THE ENERGY LOSS MODEL

To estimate the energy loss of the nitrogen ions in these plasma conditions, we use the T-Matrix framework [15],

as it had already been checked and chosen before by the experimental team.

A Boltzmann collision integral approximation is necessary for the description of short-range interactions between the projectile and the plasma electrons, including strong collisions. This is achieved using a binary collision approximation in the general kinetic equation [16]. Then, the analytic stopping power expression of the T-Matrix approximation is [15,17]

$$\frac{\partial E}{\partial x} = -\frac{n_{fe}\lambda_e^3 k_B T}{\mu^3 (2\pi)^2 v_p}\int_0^{+\infty} dp p^3 C_{bc}^T(p) \times\left[p_- \exp\left(-\frac{v_-^2}{2k_B T}\right) - p_+ \exp\left(-\frac{v_+^2}{2k_B T}\right)\right], \quad (1)$$

with $p_\pm = 1 \pm \frac{\mu k_B T}{p v_p}$ and $v_\pm = \frac{p}{\mu} \pm v_p$, where p is the projectile momentum, v_p is the projectile velocity, k_B is the Boltzmann constant, T is the electron temperature, μ is the chemical potential of the plasma, n_{fe} is the free electron density, and λ_e is electron thermal wavelength.

The calculation of the T-Matrix is limited to a spherically screened projectile Coulomb potential, i.e., to the case of static screening. Hence, the collective plasma motion is ignored. The most important factor in the expression (1) is the transport cross section $C_{bc}^T(p)$ of the scattering process of the projectile ions on the target electrons. This transport cross section depends approximately quadratically on projectile charge, Q, and can be calculated by employing the scattering phase shift method in the case of a nondegenerate plasma [15]. However, if only the first Born approximation of the transport cross section is considered, a perturbative stopping power expression can be derived which covers binary collisions in the static screening case [17].

Another possibility is to include dynamic screening and thus collective plasma excitations. This can be obtained by selecting an appropriate effective ion-electron interaction potential [18]. Alternatively, a velocity-dependent screening length can be introduced in the dynamic screening model [10,19]. The inverse velocity-dependent screening length k is defined as

$$k = k_D\left[1 + \left(\frac{v_p}{v_{th}}\right)^2\right]^{-\frac{1}{2}}, \quad (2)$$

where k_D is the inverse Debye length and v_{th} is the thermal velocity of the plasma electrons. Using this velocity-dependent screening length in the dynamic screening model, the transport cross section in the equation (1) becomes $C_{bc}^T(p, \lambda(v_p))$.

Finally. the energy loss is calculated with Eq. (1):

$$\Delta E = -\int \frac{\partial E}{[\rho(x)\partial x]}[\rho(x)dx], \quad (3)$$

where the stopping power is expressed as an energy loss per unit of areal density.

III. OUR CHARGE STATE MODEL

To estimate the projectile mean charge, each projectile charge state is simulated along the trajectory using our charge model [20] based on cross sections that solve Eqs. (4) and (5):

$$\frac{dP_q(t)}{dt} = C_{q+1}P_{q+1}(t) + L_{q-1}P_{q-1}(t) - (C_q + L_q)P_q(t), \quad (4)$$

$$Q(t) = \langle q(t)\rangle = \sum_{q=0}^{Z_p} qP_q(t), \quad (5)$$

where Z_p is the projectile atomic number, P_q is the proportion of ions with charge state q, C_q is the electron capture rate, and L_q is the electron loss rate.

$$L_q \equiv \alpha(q \to q+1), \quad (6)$$

$$C_q \equiv \alpha(q \to q-1). \quad (7)$$

Loss and capture rates, α, represent all possible electron loss and capture processes; however, due to the high predominance of monoelectron processes, these will be the only ones considered in this work. Any rate is defined as

$$\alpha_i = \sigma_i n_i v_p, \quad (8)$$

where σ_i is the cross section, n_e is the electron, and n_i is the ion density (depending on the case).

IV. CROSS SECTIONS AND RATES

In this section, we will estimate different cross sections and rates related to the considered more relevant electron loss and capture processes.

A. Ionization due to plasma ions (BEM)

The Binary Encounter Model (BEM) corresponds to the loss of a projectile electron X^{q+} due to the projectile collision with a plasma ion A^{p+}. It is described as

$$X^{q+} + A^{p+} \longrightarrow X^{(q+1)+} + A^{p+} + e^-. \quad (9)$$

This model was originally proposed by Gryzinsky [21] and has been quite successful due to its calculation simplicity; however, the main disadvantage of this model is its lack of precision for low projectile energies. For this reason, several authors have proposed improvements on this model to solve this inconvenience [22]. In this work, we use the model proposed by Kaganovich [23] since it is valid for any velocity range, which allows great simplicity in its calculation. Then, the ionization cross section due to plasma ions is calculated as

$$\sigma_{\mathrm{BEM}} = \sigma_{0,\mathrm{BEM}} \sum_{nl} \frac{N_{nl}}{Z_t^* + 1}\left(\frac{Z_t^*}{U_{nl}}\right)^2 K\left(\frac{v_p}{v_{nl}\sqrt{Z_t^* + 1}}\right), \quad (10)$$

with

$$K(x) = \frac{\exp(-1/x^2)}{x^2}[1.26 + 0.283\ln(2x^2 + 25)], \quad (11)$$

$$v_{nl} = \sqrt{2\frac{U_{nl}}{m_e}}, \quad (12)$$

$$\sigma_{0,\mathrm{BEM}} = 6.56 \times 10^{-14}\ (\mathrm{cm}^2\,\mathrm{eV}^2). \quad (13)$$

In this equation N_{nl} indicates the projectile bound electron number in shell nl. U_{nl} is its binding energy, m_e is the electron mass, Z_t^* is the effective plasma charge state, considering possible shielding effects, and v_{nl} is the bound electron orbital velocity in the nl shell.

Finally, the ionization rate due to this process can be obtained:

$$\alpha_{\mathrm{BEM}} = \sigma_{\mathrm{BEM}} v_p n_i. \quad (14)$$

B. Ionization due to plasma free electrons (FE)

Here we consider the loss of one projectile electron due to the collision with a plasma free electron:

$$X^{q+} + e^- \longrightarrow X^{(q+1)+} + 2e^-. \quad (15)$$

We use the theory developed by Lotz [24], described as

$$\sigma_{\mathrm{FE}} = \sigma_{0,\mathrm{FE}} \sum_{nl} N_{nl} \frac{\ln(E_r/U_{nl})}{E_r U_{nl}} \theta(E_r - U_{nl}), \quad (16)$$

where

$$\theta(x) = \frac{|x| + x}{2x}, \quad (17)$$

$$E_r = \frac{m_e v_r^2}{2},\ v_r = \sqrt{v_p^2 + v_{th}^2},\ v_{th} = \sqrt{\frac{k_B T}{m_e}}, \quad (18)$$

$$\sigma_{0,\mathrm{FE}} = 4 \times 10^{-14}\ (\mathrm{cm}^2\,\mathrm{eV}^2). \quad (19)$$

The $\theta(x)$ is the step function which is equal to 1 if $x > 0$ and 0 if $x \leqslant 0$ and $\sigma_{0,\mathrm{FE}}$ is a constant. E_r and v_r are the relative kinetic energy and relative velocity of the projectile electrons with respect to the plasma electrons. The relative velocity is equivalent to the geometric mean between the projectile velocity and the plasma electron thermal velocity.

It can be noticed that if the relative kinetic energy is less than the binding energy of the projectile electrons, the ionization cannot take place. Conversely, if the relative kinetic energy is higher, ionization occurs.

Then, this ionization rate is

$$\alpha_{\mathrm{FE}} = \sigma_{\mathrm{FE}} v_p n_{fe}. \quad (20)$$

C. Radiative electron capture (REC)

The radiative electron capture process consists on the capture of a plasma free electron by the projectile with higher energy than the projectile energy level where is captured. The difference in energy is released through a photon, $\hbar\omega = E_n - E_{n'}$, where E_n is the energy in the n shell, $\hbar$ is the reduced Planck constant, and ω is the photon frequency. This process is described as follows:

$$X^{q+} + e^- \longrightarrow X^{(q-1)+} + \hbar\omega. \quad (21)$$

For the calculation of this capture rate, we have used the model based on Ref. [25], which is described as

$$\alpha_{\mathrm{REC}} = \frac{2^6}{3}\left(\frac{\pi}{3}\right)^{1/2} a_0^2 \alpha_S^4 c n_{fe} Z_t Q^2 \frac{0.78}{v_p} \frac{X_v^{0.3}}{1 + X_v^2}, \quad (22)$$

where

$$X_v = \frac{v_p}{v_m} \simeq \frac{v_p}{Q}\left(\frac{3(Z_p - Q)}{2}\right)^{1/3}, \quad (23)$$

α_S is the fine structure constant, a_0 is Bohr radius, c is the speed of light in vacuum, Z_t is the plasma atomic number, and X_v is the correlation between the projectile velocity and the orbital velocity v_m of the outermost bound electron, according to Lamb-Bohr [26]. This expression does not come directly from an analytical expression; it is the result of an approximation of the model proposed by Seaton [27]. This approximation is beneficial in view of its greater simplicity and its sufficient accuracy.

D. Three-body recombination (3BR)

This recombination process can take place in plasmas with high free electron density. It occurs when the projectile simultaneously interacts with two electrons, capturing one of them and transmitting the excess energy to the other. The excess energy comes from the energy state variation of the captured electron. This process can be described as follows:

$$X^{q+} + e^- + e^- \longrightarrow X^{(q-1)+} + e^-. \quad (24)$$

To define this capture ratio, Zeldovich and Raizer developed the following expression from Thomsom's classical theory [28]:

$$r_{3\mathrm{BR}} = r_{0,3\mathrm{BR}} \frac{Q^3}{(v_r/\alpha_S c)^9}, \quad (25)$$

with

$$r_{0,3\mathrm{BR}} = 2.92 \times 10^{-31}\ (\mathrm{cm}^3/\mathrm{s}). \quad (26)$$

From this ratio, the capture rate can be calculated simply by multiplying by free electron density:

$$\alpha_{3\mathrm{BR}} = r_{3\mathrm{BR}} n_{fe}. \quad (27)$$

E. Charge transfer (CT)

The charge transfer process consists of the capture of a plasma bound electron by the projectile. To describe this process, we start from the classical theory Oppenheimer-Brinkman-Kramers (OBK) [29,30] in which, according to Betz [31] and following the sum rules of May [32], resulting the rate is

$$\alpha_{\mathrm{CT}} = \frac{2^{18}}{5}\pi a_0^2 \alpha_S c n_{be} v_p \sum_{n_i}\sum_{n_f} N_i\left(1 - \frac{N_f}{2n_f^2}\right) \times a_{eik} \frac{Q^2 U_i^{(5/2)} U_f^{(3/2)} E_k^4}{\left[E_k^2 + 2E_k(U_i + U_f) + (U_i - U_f)^2\right]^5}, \quad (28)$$

where n_{be} is the plasma bound electron density, n_i and n_f are the principal quantum numbers of the transferred electron in the initial and the final state, respectively, U_i and U_f are the

positive binding energies in these states, N_i and N_f are their occupation numbers, $E_k = v_p^2$, and a_{eik} is a reduction factor. In the classical OBK theory, $a_{eik} = 1$; however, this value ignores the possibility that the plasma recovers the electron transferred to the projectile. To consider these cases, Eichler developed an eikonal theory [33] where the a_{eik} factor was calculated as follows:

$$a_{eik} = \frac{\pi\eta v_i}{\sinh(\pi\eta v_i)}\exp\left[-2\eta v_i \arctan\left(\frac{0.5v_p - \epsilon\eta}{v_i}\right)\right] \times\left[\frac{23}{48} + \left(\frac{1}{6}v_i^2 + \frac{5}{6}\epsilon\right)\eta^2 + \frac{5}{12}\epsilon^2\eta^4\right], \tag{29}$$

$$\eta = \alpha_S c/v_p, \epsilon = (U_f - U_i)/(1\ \text{Ry}), v_i = [U_i/(1\ \text{Ry})]^{1/2},$$

where Ry is the Rydberg constant. This new a_{eik} has values between 0.1 and 0.4, and thus the effective capture section is reduced compared to the classical OBK theory.

Subsequently, Peter [25] developed a simplified model for the charge transfer capture rate, chosen in this work due to its simplicity:

$$\alpha_{\text{CT}} = \frac{2^{17}}{45}a_{eik}\pi a_0^2\alpha_S c n_{be}\frac{Q^3}{v_p^9}\varphi(Z_t, v_p), \tag{30}$$

with

$$\varphi(Z_t, v_p) = \sum_{nl}\frac{N_{nl}v_{nl}^5}{[1 + 0.5(v_{nl}/v_p)^2]^9}. \tag{31}$$

Here $\varphi(Z_t, v_p)$ is a function that depends on the plasma atomic number and the projectile velocity. In this simplified model, Peter takes the approximate constant value of 0.15 for a_{eik}.

F. Dielectronic recombination (DR)

The dielectronic recombination consists in a process of two phases. First, a free electron is captured by the projectile, and the energy difference between the free state and the captured state in the nl_k shell is transferred to another bound electron in a lower nl_i shell. This energy transmission causes the electron of the nl_i shell to excite up to an upper nl_j shell, such that

$$X^{q+} + e^- \longrightarrow X^{**(q-1)+}. \tag{32}$$

The atom, in its excited state X^{**}, will tend to stabilize by a radiative decay of the excited electron $X(nl_i \rightarrow nl_j)$. In this step, the energy excess is released by a photon $\hbar\omega = E_{nl_i} - E_{nl_j}$, returning to a ground state:

$$X^{**(q-1)+} \longrightarrow X^{*(q-1)+} + \hbar\omega; \tag{33}$$

on the other hand, the electron captured in the nl_k shell remains in that excited state, although it will tend to decay to lower shells over time.

For this recombination rate, a model developed by Peter [34,35] has been used, which is defined as

$$\alpha_{\text{DR}} = \frac{h^3 n_{fe}}{(2\pi m_e v_{th}^2)^{3/2}}\sum_{nl_i}\sum_{nl_j}\sum_{nl_k}N_{nl_i}\frac{2(2l_j+1) - N_{nl_j}}{2(2l_j+1)} \times(2l_k+1)\frac{A_r^{(1)}A_a^{(1)}}{A_r^{(1)} + A_a^{(1)}}F(s,t), \tag{34}$$

where

$$F(s,t) = \frac{\exp[-(s-t)^2] - \exp[-(s+t)^2]}{4st},$$
$$s = \sqrt{\frac{E_{nl_j} - E_{nl_i} + E_{nl_k}}{k_B T}}, t = \sqrt{\frac{m_e v_p^2}{2k_B T}}. \tag{35}$$

Here h is the Planck constant, N_{nl_i} and N_{nl_j} are the occupation numbers of the N_{nl_i} and N_{nl_j} shells, respectively, and E_{nl_i}, E_{nl_j}, and E_{nl_k} are, respectively, the binding energy of the electrons in the shells nl_i, nl_j, and nl_k. On the other hand, $A_r^{(1)}$ and $A_a^{(1)}$ are radiative stabilization and self-ionization rates, respectively, defined as

$$A_r^{(1)} = \frac{1\ \text{Ry}}{\hbar}\alpha_S^3\left(\frac{E_{nl_j} - E_{nl_i}}{1\ \text{Ry}}\right)^2 f^{(1)}(j \rightarrow i), \tag{36}$$

$$A_a^{(1)} = \frac{8}{\sqrt{3}}\frac{1\ \text{Ry}}{\hbar}\frac{Q^2}{n^3}\frac{1\ \text{Ry}}{E_{nl_i} - E_{nl_j}}\frac{f^{(1)}(j \rightarrow i)}{2l+1} \times\frac{0.4\sqrt{d/\pi}}{2 - \exp\left(\frac{-0.6}{n_k^{\frac{4}{3}} d^{\frac{1}{2}}}\right)}\exp[-d(l - l_p)^2], \tag{37}$$

with

$$d = \frac{\sqrt{1+y}}{2.5n_k}, l_p = n_k^{2/3}\sqrt{1+y}, y = \frac{n_k^2 m_e v_p^2}{2Q^2}. \tag{38}$$

Furthermore, $f^{(1)}(j \rightarrow i)$ is the oscillation strength between nl_j and nl_i shells.

It is important to note that these definitions do not consider the self-ionization processes of the valence electrons. The relevance of these processes within dielectronic recombination is discussed in Ref. [34] as well as in more publications [36]. To consider this, a new valence self-ionization rate $A_v^{(1)}$ should be introduced in Eq. (34),

$$\frac{A_r^{(1)}A_a^{(1)}}{A_r^{(1)} + A_a^{(1)}} \longrightarrow \frac{A_r^{(1)}A_a^{(1)}}{A_r^{(1)} + A_a^{(1)} + A_v^{(1)}}. \tag{39}$$

In general, the self-ionization processes of the valence electrons are only of interest in cases with fast projectiles with high Z_p and low charge state q and which therefore have a high number of electrons in their valence shell. In these cases, there is a reduction in the electron capture rate of approximately two orders of magnitude. However, in this work, we do not use this self-ionization rate as it is not the case mentioned before and the accuracy is already sufficient by using a simpler model. This rate is relevant when we are working with heavy projectiles at high kinetic energies (1–10 MeV/u) and at medium-low charge states.

Finally, once the ionization and recombination rates have been described, it is possible to calculate the total rates as

$$L_q = \alpha_{\text{BEM}} + \alpha_{\text{FE}}, \tag{40}$$

$$C_q = \alpha_{\text{REC}} + \alpha_{\text{3BR}} + \alpha_{\text{CT}} + \alpha_{\text{DR}}. \tag{41}$$

V. RESULTS

A. Charge state

Figures 1–3 show the average projectile charge state of a nitrogen projectile along with the plasma parameters at three

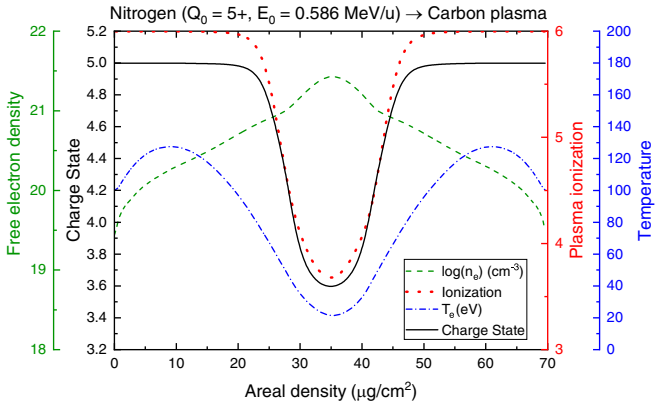

FIG. 1. Carbon plasma parameters at 3 ns and nitrogen charge state

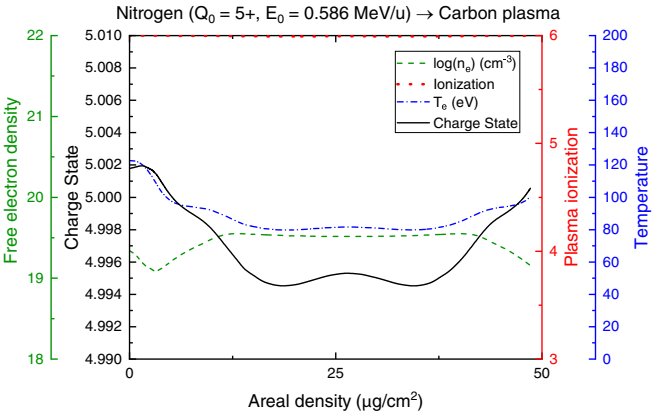

FIG. 3. Carbon plasma parameters at 12 ns and nitrogen charge state.

different times (3, 7, and 12 ns) to illustrate the effect of the plasma conditions on the projectile charge state in both partially and fully ionized plasma.

Initial nitrogen energy is $E_0 = 0.586$ MeV/u, measured after it passes through the degrader where it achieves an average charge state of $Q_0 = 5.05+$, according to ETACHA calculations [37], which is the initial charge of the projectile prior to its interaction with the laser-generated carbon plasma.

Figure 1 illustrates the average charge state at 3 ns from the onset of the laser pulse. At this instant, the carbon plasma generated by the laser is partially ionized, achieving an ionization of about 3.5+ at the plasma center. This instant shows the largest variation of the charge state across the areal density due to the nonuniform ionization throughout the ion trajectory. Here we plainly see that, for the plasma parameters considered, partial ionization of the target leads to a decrease in the projectile charge state because bound electron capture is the dominant process. This plasma profile across the areal density results in a considerable variation in the charge state of the projectile from 5.0+ to 3.6+ at the center. The reason is that a higher bound electron density in the target yields an increase in the recombination rate of the nonradiative process.

In contrast, Fig. 2 illustrates the average charge state at 7 ns from the onset of the laser pulse, when the carbon plasma

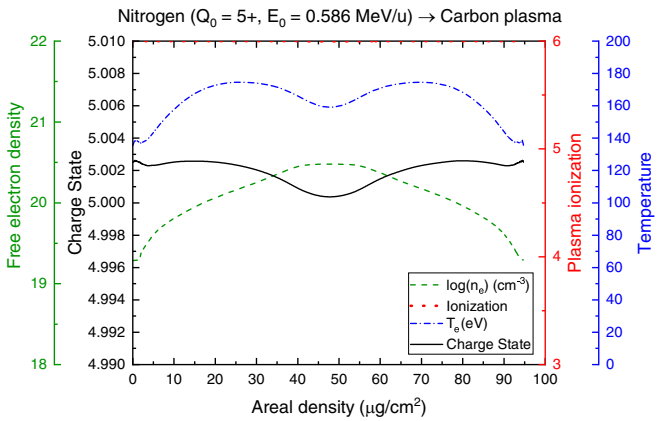

FIG. 2. Carbon plasma parameters at 7 ns and nitrogen charge state.

generated by laser is almost totally ionized. It reveals a slight variation in the projectile charge state because of the slight variation in the high ionization of the target. In this case, the charge state is varied only from 5.003+ to 5.000+ across the areal density because nonradiative recombination is significantly decreased and radiative recombination is the dominant capture process.

Lastly, Fig. 3 illustrates the equilibrium charge state at 12 ns from the onset of the laser pulse. At this instant, the carbon laser-generated plasma is also almost totally ionized, but with a small fraction of bound electrons (greater than in the case at 7 ns). The projectile average charge state behavior is also similar to the last case, exhibiting a higher variation from 5.002+ to 4.994+. This reveals the influence of a small portion of bound electrons in this experiment, resulting in a charge state lower than the cold matter due to the so-called density effect. This effect involves the reduction of radiative capture since, at higher densities, the probability of the projectile interaction with a free electron is also higher, which results in ionization of the captured electron [35].

B. Energy loss

The predictions of charge state models in the energy loss are compared with energy loss data in Fig. 4 for the nitrogen projectiles in the carbon laser-generated plasma. The energy loss is shown as a function of time and normalized to the energy loss in the solid target, which was measured being 0.85 MeV. This experiment is helpful to prove our charge state model in the low energy range from energy loss calculations. The nitrogen had an initially charged state of $Q_0 = 5.05+$ and an energy of $E_0 = 0.586$ MeV/u. Our model combines the predictions of our charge state model across the areal density (check Figs. 1–3) with the T-Matrix energy loss model. The T-Matrix model represents the nonperturbative energy loss calculation.

Figure 4 compares our theoretical calculations with those made by Cayzac *et al.* [1]. These authors utilized a Monte Carlo (MC) code and the Kreussler and Gus'kov models to determine the projectile's state of charge. They contrasted the three models and showed that only the Kreussler [11] and Gus'kov [14] models (both very similar) were comparable

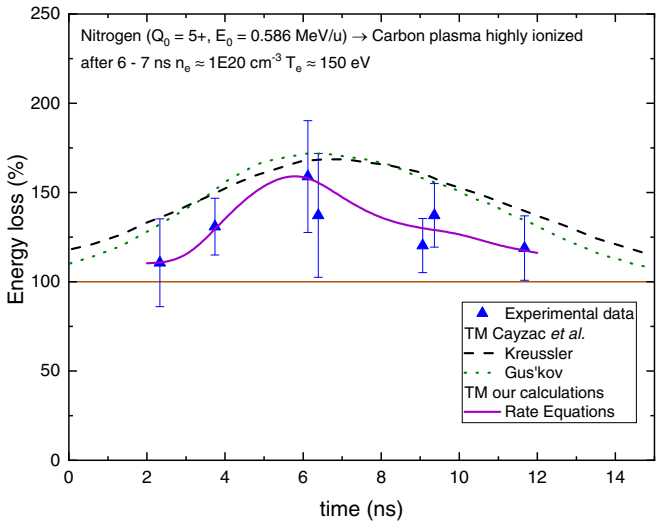

FIG. 4. Energy loss of nitrogen projectiles in carbon laser-generated plasmas as a function of time. Values are normalized to the energy loss in solid carbon.

with the measurements, so the Gus'kov model was chosen for their final results, giving a projectile charge state in the range of 5.1+ to 5.4+. Nevertheless, their predictions contrast with ours, which here are between 3.500+ at the lowest target ionization and 5.003+ at the highest target ionization.

Results shows that our theoretical predictions agree very well with the data. Here, we have made used of the same energy loss T-Matrix scheme used by the experimental team and therefore the differences in the theoretical predictions must come only from the charge state model.

VI. CONCLUSIONS

The average charge state, together with the energy loss of slow nitrogen ions, has been computed theoretically and checked against experimental data in a carbon laser-generated plasma. It is supposed that the largest disagreements between existing theories on ion stopping power arise around the maximum of the stopping power, close to the Bragg peak. For a plasma temperature around 100–200 eV, the maximum stopping power is achieved for projectile energies near 0.5–0.6 MeV/u.

Different projectile electron loss and capture processes were taken into account to estimate the projectile charge state. The electron loss, or ionization, with plasma ions and free electrons have been considered. On the other hand, the electron capture, or recombination, with plasma free or bound electrons have been also considered. The projectile ionization with plasma ions was shown as the main factor that modifies the mean charge of the projectile. Here, the new Kaganovich fitting formula for this projectile ionization was used because it seems to be more accurate than Gryzinsky's fitting in the low energy range.

The energy loss has been also calculated by using the projectile charge state profile obtained with the model described before and compared with the estimations and data of Cayzac *et al.* [1]. In view of the results, the calculation agrees very well with the data because our projectile charge model predicts a lower charge state than the one predicted by the experimental team.

To conclude, we must say that our charge state model fits better with experimental data than any other model in the bibliography. Thus, it should be considered in any charge state and any energy loss estimation, now and in the future, to obtain reliable results [20].

ACKNOWLEDGMENTS

This work was financed by the the Junta de Comunidades de Castilla La Mancha under Contract No. SBPLY/19/180501/000105. We especially acknowledge W. Cayzac for very useful data and comments.

[1] W. Cayzac, A. Frank, A. Ortner, V. Bagnoud, M. Basko, S. Bedacht, C. Bläser, A. Blažević, S. Busold, O. Deppert *et al.*, Nat. Commun. **8**, 15693 (2017).
[2] V. Bagnoud, B. Aurand, A. Blazevic, S. Borneis, C. Bruske, B. Ecker, U. Eisenbarth, J. Fils, A. Frank, E. Gaul *et al.*, Appl. Phys. B **100**, 137 (2010).
[3] A. Frank, A. Blazević, V. Bagnoud, M. M. Basko, M. Borner, W. Cayzac, D. Kraus, T. Hessling, D. H. H. Hoffmann, A. Ortner, A. Otten, A. Pelka, D. Pepler, D. Schumacher, A. Tauschwitz, and M. Roth, Phys. Rev. Lett. **110**, 115001 (2013).
[4] W. Cayzac, V. Bagnoud, M. M. Basko, A. Blažević, A. Frank, D. Gericke, L. Hallo, G. Malka, A. Ortner, A. Tauschwitz *et al.*, Phys. Rev. E **92**, 053109 (2015).
[5] A. Tauschwitz, M. Basko, A. Frank, V. Novikov, A. Grushin, A. Blazevic, M. Roth, and J. Maruhn, High Energy Density Phys. **9**, 158 (2013).
[6] G. Xu, M. Barriga-Carrasco, A. Blazevic, B. Borovkov, D. Casas, K. Cistakov, R. Gavrilin, M. Iberler, J. Jacoby, G. Loisch *et al.*, Phys. Rev. Lett. **119**, 204801 (2017).
[7] H.-K. Chung, M. Chen, W. Morgan, Y. Ralchenko, and R. Lee, High Energy Density Phys. **1**, 3 (2005).
[8] M. D. Barriga-Carrasco, L. González-Gallego, J. M. Gil, R. Rodríguez, and G. Espinosa, Phys. Plasmas **25**, 093113 (2018).
[9] C.-K. Li and R. D. Petrasso, Phys. Rev. Lett. **70**, 3059 (1993).
[10] D. O. Gericke and M. Schlanges, Phys. Rev. E **67**, 037401 (2003).
[11] S. Kreussler, C. Varelas, and W. Brandt, Phys. Rev. B **23**, 82 (1981).
[12] M. D. Barriga-Carrasco, Phys. Rev. E **88**, 043107 (2013).
[13] M. D. Barriga-Carrasco, D. Casas, and R. Morales, Phys. Rev. E **93**, 033204 (2016).
[14] S. Y. Gusâkov, N. Zmitrenko, D. Ilâin, A. Levkovskii, V. Rozanov, and V. Sherman, Plasma Phys. Rep. **35**, 709 (2009).
[15] D. O. Gericke and M. Schlanges, Phys. Rev. E **60**, 904 (1999).

[16] D. Kremp, M. Schlanges, and T. Bornath, J. Stat. Phys. **41**, 661 (1985).
[17] K. Morawetz and G. Röpke, Phys. Rev. E **54**, 4134 (1996).
[18] G. Zwicknagel, C. Toepffer, and P. G. Reinhard, Phys. Rep. **309**, 117 (1999).
[19] D. O. Gericke, M. Schlanges, and T. Bornath, Phys. Rev. E **65**, 036406 (2002).
[20] J. Braenzel, M. D. Barriga-Carrasco, R. Morales, and M. Schnürer, Phys. Rev. Lett. **120**, 184801 (2018).
[21] M. Gryziński, Phys. Rev. **138**, A305 (1965).
[22] G. H. Gillespie, Phys. Lett. A **93**, 327 (1983).
[23] I. D. Kaganovich, E. A. Startsev, R. C. Davidson, S. R. Kecskemeti, A. Bin-Nun, D. Mueller, L. Grisham, R. L. Watson, V. Horvat, K. E. Zaharakis *et al.*, Nucl. Instrum. Methods Phys. Res. Sect. A **544**, 91 (2005).
[24] W. Lotz, Z. Phys. **206**, 205 (1967).
[25] T. Peter, Laser Part. Beams **8**, 643 (1990).
[26] W. E. Lamb, Phys. Rev. **58**, 696 (1940).
[27] M. Seaton, Mon. Not. R. Astron. Soc. **119**, 81 (1959).
[28] Y. B. Zel'Dovich and Y. P. Raizer, *Physics of Shock Waves and High-Temperature Hydrodynamic Phenomena* (Courier Corporation, 2002).
[29] J. R. Oppenheimer, Phys. Rev. **31**, 349 (1928).
[30] H. Brinkmann and H. Kramers, Proc. K. Ned. Akad. Wet **33**, 973 (1930).
[31] H. D. Betz, Heavy ion charge states, *Condensed Matter*, Applied Atomic Collision Physics Vol. 4 (Academic Press, 1983), pp. 1–42.
[32] R. M. May, Phys. Rev. **136**, A669 (1964).
[33] J. Eichler and F. T. Chan, Phys. Rev. A **20**, 104 (1979).
[34] T. Peter, R. Arnold, and J. Meyer-ter-Vehn, Phys. Rev. Lett. **57**, 1859 (1986).
[35] T. Peter and J. Meyer-ter-Vehn, Phys. Rev. A **43**, 1998 (1991).
[36] C. Deutsch and G. Maynard, Matter Radiat. Extremes **1**, 277 (2016).
[37] J. P. Rozet, C. Stéphan, and D. Vernhet, Nucl. Instrum. Methods Phys. Res. Sect. B **107**, 67 (1996).